31st Annual International Conference of the IEEE EMBS
Minneapolis, Minnesota, USA, September 2-6, 2009

Detection of Architectural Distortion in Prior Mammograms of Interval-cancer Cases with Neural Networks

Shantanu Banik, Rangaraj M Rangayyan*, and J. E. Leo Desautels
Department of Electrical and Computer Engineering, Schulich School of Engineering, University of Calgary
2500 University Drive NW, Calgary, Alberta, Canada, T2N 1N4. *ranga@ucalgary.ca.

Abstract— **Architectural distortion is a commonly missed sign of breast cancer. This paper investigates the detection of architectural distortion, in mammograms of interval-cancer cases taken prior to the diagnosis of breast cancer, using Gabor filters, phase portrait analysis, fractal dimension, and texture analysis. The methods were used to detect initial candidates for sites of architectural distortion in prior mammograms of interval-cancer and also normal cases. A total of 4212 regions of interest (ROIs) were automatically obtained from 106 prior mammograms of 56 interval-cancer cases, including 262 ROIs related to architectural distortion, and from 52 prior mammograms of 13 normal cases. For each ROI, the fractal dimension and Haralick's texture features were computed. Feature selection was performed using stepwise logistic regression and in terms of the area under the receiver operating characteristics (ROC) curve (AUC). The best results achieved, in terms of AUC, are 0.75 with the Bayesian classifier, 0.71 with Fisher linear discriminant analysis, and 0.76 with an artificial neural network (ANN) based on radial basis functions (RBF). Analysis of the performance of the methods with free-response receiver operating characteristics indicated a sensitivity of 0.80 at 10.5 false positives per image.**

I. Introduction

Early detection of breast cancer is crucial if treatment is to be successful. Mammography is the best available tool for early detection of breast cancer. However, the sensitivity of screening mammography is influenced by image quality and the radiologist's level of expertise. Computer-aided diagnosis (CAD) could help in increasing the detection accuracy by providing a "second opinion" to the radiologist, and could be as effective as double reading [1].

Architectural distortion is the third most common mammographic sign of non-palpable breast cancer, but due to its subtlety and variability in presentation, it is often missed during screening [2]. CAD techniques and systems are effective in detecting masses and microcalcifications [3]. However, only a few works have been reported on the detection of architectural distortion [4], [5], [6], [7], [8], and CAD systems have been found to fail in detecting architectural distortion with an adequate level of accuracy [3].

Ayres and Rangayyan [4] applied Gabor filters and phase portrait maps to characterize the oriented patterns associated with architectural distortion. Matsubara et al. [5] used mathematical morphology to detect architectural distortion around the skin line and a concentration index to detect architectural distortion within the mammary gland. Guo et al. [6] used five different methods to estimate the fractal dimension (FD) and a support vector machine (SVM) for classification of masses and architectural distortion. Rangayyan et al. [7] used phase portraits, FD, and texture features for the detection of architectural distortion in prior mammograms of screen-detected cancer. Sameti et al. [8] used six selected texture and photometric features computed from manually marked regions on the last screening mammograms prior to the detection of breast cancer.

In this paper, we present methods for the detection of sites of architectural distortion in prior mammograms of interval-cancer cases in a screening program. The methods are based upon Gabor filters, phase portrait modeling, fractal analysis, and Haralick's texture features.

II. Methods

After performing the segmentation of the breast portion in a given mammogram, the method for the detection of architectural distortion consists of the following stages: extraction of the orientation field using Gabor filters, selection of curvilinear structures (CLS), filtering and downsampling of the orientation field, modeling of phase portraits, and detection of potential sites of architectural distortion [4], [7].

A. Gabor Filters for the Detection of Oriented Patterns

The real Gabor filter kernel oriented at the angle $\theta = -\pi/2$ is given by [9], [10]

$$g(x,y) = \frac{1}{2\pi\sigma_x\sigma_y} \exp\left[-\frac{1}{2}\left(\frac{x^2}{\sigma_x^2} + \frac{y^2}{\sigma_y^2}\right)\right] \cos(2\pi f x). \quad (1)$$

Kernels at other angles can be obtained by rotating this kernel. In the present work, the parameters in Equation 1, namely σ_x, σ_y, and f, were derived using the design rules proposed by Rangayyan and Ayres [10]. A set of 180 kernels with angles spaced evenly over the range [-$\pi/2$, $\pi/2$] was used. For each image, a magnitude response and orientation field were obtained by using the response and angle of the Gabor filter with the highest response at each pixel. The CLS of interest (spicules and fibroglandular tissue) were separated from confounding structures (edges of the pectoral muscle and parenchymal tissue, breast boundary, and noise) using the orientation field, the gradient field, and the nonmaximal suppression technique [4]. The selected core CLS pixels and

This work was supported by the Canadian Breast Cancer Foundation (CBCF): Prairies/NWT Chapter and the Natural Sciences and Engineering Research Council (NSERC) of Canada.

the orientation field were filtered and downsampled to reduce noise and computational requirements.

B. Phase Portrait Analysis

The phase portrait diagram of a system of two linear, first-order, differential equations depicts the possible trajectories of the state variables for different initialization values [11]. Let $p(t)$ and $q(t)$, $t \in \mathbb{R}$, denote two differentiable functions of time t, related as $\dot{p}(t) = F[p(t), q(t)]$ and $\dot{q}(t) = G[p(t), q(t)]$, where $\dot{p}(t)$ and $\dot{q}(t)$ indicate the first-order derivatives with respect to time, and F and G represent functions of p and q [10]. Given initial conditions $p(0)$ and $q(0)$, the solution $(p(t), q(t))$, can be viewed as a parametric trajectory or streamline of a hypothetical particle in the (p, q) plane placed at $(p(0), q(0))$, at time $t = 0$, and moving through the (p, q) plane with the velocity $(\dot{p}(t), \dot{q}(t))$. The (p, q) plane is referred to as the phase plane of the system; the phase portrait is a graph of the possible streamlines in the phase plane. A fixed point is a point in the phase plane where $\dot{p}(t) = 0$ and $\dot{q}(t) = 0$; a particle left at a fixed point remains stationary. When the system is affine, $[\dot{p}(t), \dot{q}(t)]^T = \mathbf{A}[p(t), q(t)]^T + \mathbf{b}$, where $\mathbf{A}$ is a 2×2 matrix and $\mathbf{b}$ is a 2×1 column matrix. The center (p_0, q_0) of the phase portrait is given by the fixed point as $[\dot{p}(t), \dot{q}(t)]^T = 0 \Rightarrow [p_0, q_0]^T = -\mathbf{A}^{-1}\mathbf{b}$. Associating the functions $p(t)$ and $q(t)$ with the x and y co-ordinates of the Cartesian (image) plane, we can define the orientation field as $\phi(x, y|\mathbf{A}, \mathbf{b}) = \arctan(\dot{q}(t)/\dot{p}(t))$, which is the angle of the velocity vector $(\dot{p}(t), \dot{q}(t))$ with the x axis at (x, y)=$(p(t), q(t))$.

In the model described above, there are three types of phase portraits: node, saddle, and spiral; they can be determined from the nature of the eigen values of $\mathbf{A}$. Because spiral patterns are not of interest in the present work, the matrix $\mathbf{A}$ was constrained to be symmetric, resulting in two phase portrait maps: node and saddle. Because a mammogram could exhibit several patterns, a sliding analysis window of size 10×10 pixels was used with one pixel per step. For each position of the window a vote was cast at the node position given by the corresponding fixed point. The peaks in the node map are expected to indicate the sites of architectural distortion.

C. Experimental Setup and Database

In this study, 52 mammographic images of 13 normal individuals and 106 mammographic images of 56 individuals diagnosed with breast cancer were selected from a database of 1,745 digitized mammograms of 170 subjects obtained from Screen Test: Alberta Program for the Early Detection of Breast Cancer. The film mammograms were digitized at the spatial resolution of 50 μm and gray-scale resolution of 12 bits/pixel. Mammograms acquired in the last scheduled visit to the screening program prior to the detection of cancer were included in the dataset for the present study, and labeled as "prior mammograms". The term "interval cancer" is used to indicate a case where breast cancer was detected outside the screening program in the interval between scheduled screening sessions. The mammograms on which cancer was detected were not available for the present study. All prior mammograms had been declared to be free of signs of breast cancer at the time of their original acquisition and interpretation in the screening program. The normal control cases selected represent the penultimate screening visits at the time of preparation of the database, and hence are considered to be prior mammograms for the normal cases also. The images were filtered and downsampled to 200 μm/pixel and 8 bits/pixel before applying the Gabor filters. The orientation field was filtered and downsampled to an effective resolution of 800 μm/pixel to facilitate efficient phase portrait modeling.

The 106 prior mammograms of interval-cancer cases were reviewed by a radiologist specialized in screening mammography (J.E.L.D.). Regions related to or suspected to contain architectural distortion were marked using rectangular boxes based on the reports available on subsequent imaging, or biopsy, or by detailed inspection of the prior mammograms. The images were divided into two categories: visible architectural distortion (38 images) and questionable or no visible architectural distortion (68 images). From the 158 mammograms in the study, a total of 4212 ROIs (2821 ROIs from interval-cancer cases with 262 ROIs related to the sites of architectural distortion, and 1391 ROIs from the normal cases) of size 128×128 pixels (except at the edges of the images) were automatically obtained. ROIs were labeled at the locations indicated by the peaks in the node maps, in decreasing order of the value of the peak, up to a maximum of 30 ROIs per mammogram. The ROIs with their centers within the areas of architectural distortion identified by the radiologist were labeled as true-positive ROIs; the others were labeled as false-positive ROIs. Phase portrait analysis did not detect any true-positive ROI in 14 prior mammograms of the interval-cancer cases; the radiologist had indicated that the corresponding images had no visible architectural distortion.

The results of application of the methods are illustrated in Figure 1 for a prior mammogram of an interval-cancer case. In part (a), the rectangle shows the area of architectural distortion identified by the radiologist. The magnitude image resulting from the Gabor filters, the orientation field, and the node map are shown in parts (b), (c), and (d), respectively. A peak is evident at the site of architectural distortion. Figure 1 (e) shows the ROIs obtained.

D. Feature Extraction

Haralick's statistical measures of texture [12], based on the gray-level co-occurrence matrix (GCM), were used in the present work. Four normalized GCMs were computed with unit pixel distance for the angles of $0, 45, 90$, and 135 degrees. The four GCMs were averaged to obtain a single GCM for computation of Haralick's 14 texture features.

The two-dimensional (2D) Fourier spectrum of each ROI was transformed into a one-dimensional (1D) function $S(f)$, by averaging as a function of the radial distance f from the zero-frequency point over all angles. The spectrum $S(f)$ is related to the radial frequency f according to the model

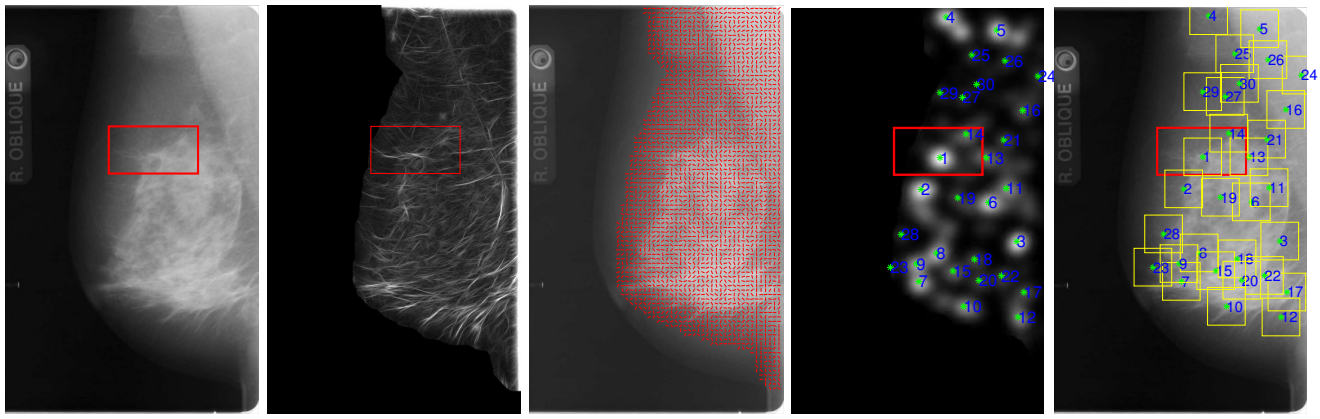

(a) (b) (c) (d) (e)

Fig. 1. (a) The "prior mammogram" of an interval cancer case. The rectangle is of size 59.9 mm × 31.7 mm, and indicates the region of architectural distortion. Image size 1370 × 850 pixels at 200 μm per pixel. (b) Magnitude response obtained using a bank of 180 real Gabor filters. (c) Orientation field angle superimposed on the mammographic image; needles are drawn for every fifth pixel. (d) The node map. Each asterisk mark (*) corresponds to a peak position detected automatically in the node map. The numbers next to the asterisk marks indicate the peaks in descending order of magnitude. (e) The 30 ROIs obtained automatically using the peaks detected in the node map. The size of each ROI is 128 × 128 pixels (except at the edges).

$S(f) \propto (1/f)^{\beta}$. Linear regression was applied to a limited frequency range of the 1D spectrum plotted on a log-log scale, excluding points in the low-frequency and high-frequency regions, to estimate the slope β of the fitted line. β is related to FD as [13] FD $= (8 - \beta)/2$.

E. Feature Selection

Feature selection was performed separately based on stepwise logistic regression, sequential forward selection, and the area under the receiver operating characteristics (ROC) curve (AUC) for each feature. The t-test was also applied to obtain the p-value to evaluate the statistical significance of the difference between the values of a given feature for the true-positive and false-positive ROIs. Logistic regression resulted in selection of the six features sum average, entropy, node value, contrast, FD, and correlation. Sequential forward selection led to the five features sum average, node value, difference variance, energy, and FD. The top five features in terms of AUC (with p-value < 0.001) were sum average, node value, difference variance, contrast, and FD. The features selected by stepwise regression and the top five features selected based on AUC were used for classification.

F. Pattern Classification

The ROC and the free-response receiver operating characteristics (FROC) procedures were used to test and evaluate the classification accuracy using several classifiers. For ROC analysis, Fisher linear discriminant analysis (FLDA); the Bayesian method; and the artificial neural network (ANN) based on the single-layer perceptron (SLP) with a tangent sigmoid activation function, the multi-layer perceptron (MLP) with two hidden layers (the first hidden layer with three neurons and the second with one neuron) and tangent sigmoid activation function, and radial basis functions (RBF) [14] were used. In training and testing the FLDA and Bayesian classifiers, the leave-one-out (LOO) method was used. For classification using ANNs with SLP, MLP, and RBF, 50% of each of the true-positive and the false-positive ROIs were randomly selected to generate the training and the testing sets, and the procedure was repeated 50 times. FROC analysis was used to assess the false-positive rate for a given level of sensitivity when classification of the ROIs was placed in the context of detection of architectural distortion in full mammograms. The generalized regression neural network (GRNN) and the ANN based on SLP, MLP, and RBF were used for classification using the LOO method: the features of all ROIs belonging to the image being analyzed were removed from the dataset when training the classifier.

III. Results and Discussion

The ROC performance achieved, in terms of the AUC, is presented in Table I using the features selected by stepwise logistic regression and the top five features obtained by ROC analysis. With ANN-based classification, the results were expected to be better compared to the FLDA and Bayesian methods. However, because of resampling for cross-validation, the results are biased, and highly dependent on the sample size, the randomly selected samples, and their statistical distribution [15]. Furthermore, the AUC obtained based on crossvalidation and with ANN-based classifiers are pessimistically biased because the ratio of the total number of available samples per class to the number of available features is greater than five [15]. The results could be improved by using the LOO method with these classifiers.

The results of FROC analysis are presented in Table II for several classifiers with the leave-one-image-out method. The FROC curves using four classifiers with the six features obtained by stepwise logistic regression are shown in Figure 2. With the sensitivity of 0.8 as the reference point, the selected features showed the best performance of 10.5 false positives per image using ANN-RBF.

Ayres and Rangayyan [4] achieved a sensitivity of 95% at

TABLE I

RESULTS OBTAINED IN TERMS OF AUC USING THE SELECTED FEATURES BASED ON STEPWISE LOGISTIC REGRESSION AND ROC ANALYSIS. STD.= STANDARD DEVIATION.

Classifier	Six features from stepwise logistic regression	Top five features based on ROC analysis
FLDA	0.71	0.69
Bayesian	0.75	0.74
SLP	mean 0.72, std. 0.03	mean 0.71, std. 0.06
MLP	mean 0.74, std. 0.08	mean 0.73, std. 0.10
RBF	mean 0.75, std. 0.03	mean 0.76, std. 0.03

9.9 false positives per image. Rangayyan et al. [7] obtained a sensitivity of 79% at 8.4 false positives per image. In the work reported by Sameti et al. [8] the average classification rate was 72%. Compared to those, the results obtained in the current work are significant and encouraging.

TABLE II

RESULTS OBTAINED USING SEVERAL CLASSIFIERS AND THE LEAVE-ONE-IMAGE-OUT METHOD IN FROC ANALYSIS. THE RESULTS ARE IN TERMS OF FALSE POSITIVES PER IMAGE AT 80% SENSITIVITY.

Classifier	Six features from stepwise logistic regression	Top five features based on ROC analysis
GRNN	11.3	11.5
SLP	13.3	11.9
MLP	12.1	13.6
RBF	10.5	10.8

IV. CONCLUSION

The results obtained with the prior mammograms of interval-cancer cases, including a set of normal control cases, and without incorporating the mammograms on which cancer was detected, are comparable to the results obtained by Rangayyan et al. [7], [16] using smaller sets of images, different feature selection technique, and other classifiers. Even with a larger dataset and a number of normal control cases included, there is not much increase in the number of false positives per image. In addition, there were as many as 68 images with no visible or questionable architectural distortion. The results indicate that the proposed methods can be used to achieve earlier detection of subtle signs of breast cancer in mammograms, in particular architectural distortion, with good accuracy.

The derivation of additional features for the detection of sites of architectural distortion at higher sensitivity and lower false-positive rates, and the use of the SVM as the classifier are in progress. Increased sensitivity in breast cancer diagnosis and the development of CAD techniques for localization of architectural distortion could lead to efficient detection of early signs of breast cancer.

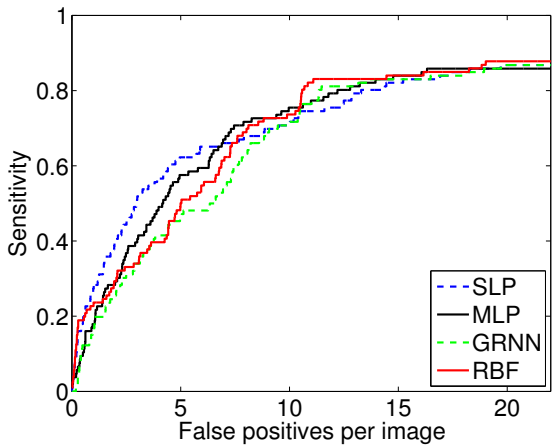

Fig. 2. FROC curves using four classification techniques with the leave-one-image-out method and the six features obtained by logistic regression.

REFERENCES

[1] K. Doi, "Computer-aided diagnosis in medical imaging: historical review, current status and future potential," *Computerized Med. Imaging and Graphics*, vol. 31, pp. 198–211, 2007.

[2] A. M. Knutzen and J. J. Gisvold, "Likelihood of malignant disease for various categories of mammographically detected, nonpalpable breast lesions," *Mayo Clinic Proc.*, vol. 68, pp. 454–460, 1993.

[3] J. A. Baker, E. L. Rosen, J. Y. Lo, E. I. Gimenez, R. Walsh, and M. S. Soo, "Computer-aided detection (CAD) in screening mammography: Sensitivity of commercial CAD systems for detecting architectural distortion," *American J. Roentgenology*, vol. 181, pp. 1083–1088, 2003.

[4] F. J. Ayres and R. M. Rangayyan, "Reduction of false positives in the detection of architectural distortion in mammograms by using a geometrically constrained phase portrait model," *Intl. J. Computer Assisted Radiology and Surgery*, vol. 1, pp. 361–369, 2007.

[5] T. Matsubara, T. Ichikawa, T. Hara, H. Fujita, S. Kasai, T. Endo, and T. Iwase, "Automated detection methods for architectural distortions around skinline and within mammary gland on mammograms," in *Proc. the 17th Intl. Congress and Exhibition on Computer Assisted Radiology and Surgery*, H. U. Lemke, M. W. Vannier, K. Inamura, A. G. Farman, K. Doi, and J. H. C. Reiber, Eds., London, UK, 2003, pp. 950–955, Elsevier.

[6] Q. Guo, J. Shao, and V. F. Ruiz, "Characterization and classification of tumor lesions using computerized fractal-based texture analysis and support vector machines in digital mammograms," *Intl. J. Computer Assisted Radiology and Surgery*, vol. 4(1), pp. 11–25, 2009.

[7] R. M. Rangayyan, S. Prajna, F. J. Ayres, and J. E. L. Desautels, "Detection of architectural distortion in mammograms acquired prior to the detection of breast cancer using Gabor filters, phase portraits, fractal dimension, and texture analysis," *Intl. J. Computer Assisted Radiology and Surgery*, vol. 2(6), pp. 347–361, 2008.

[8] M. Sameti, R. K. Ward, J. M.-Parkes, and B. Palcic, "Image feature extraction in the last screening mammograms prior to detection of breast cancer," *IEEE J. Selected Topics in Signal Processing*, vol. 3(1), pp. 46–52, 2009.

[9] D. Gabor, "Theory of communication," *J. Institute of Electrical Engineers*, vol. 93, pp. 429–457, 1946.

[10] R. M. Rangayyan and F. J. Ayres, "Gabor filters and phase portraits for the detection of architectural distortion in mammograms," *Med. and Biol. Engineering and Computing*, vol. 44, pp. 883–894, 2006.

[11] A. R. Rao, *A Taxonomy for Texture Description and Identification*, Springer-Verlag, New York, NY, 1990.

[12] R. M. Haralick, "Statistical and structural approaches to texture," *Proc. IEEE*, vol. 67, pp. 786–804, 1979.

[13] M. Aguilar, E. Anguiano, and M. A. Pancorbo, "Fractal characterization by frequency analysis: II. A new method," *J. Microscopy*, vol. 172, pp. 233–238, 1993.

[14] R. O. Duda, P. E. Hart, and D. G. Stork, *Pattern Classification*, Wiley-Interscience, New York, NY, 2nd edition, 2001.

[15] B. Sahiner, H.-P. Chan, N. Petrick, R. F. Wagner, and L. Hadjiiski, "Feature selection and classifier performance in computer-aided diagnosis: the effect of finite sample size," *Medical Physics*, vol. 27(7), pp. 1509–1522, 2000.

[16] R. M. Rangayyan, S. Banik, S. Prajna, and J. E. L. Desautels, "Detection of architectural distortion in prior mammograms of interval-cancer cases," in *Proc. 23rd Intl. Congress and Exhibition: Computer Assisted Radiology and Surgery*, Berlin, Germany, 2009, In press.